Journal of Glaciology

Witnessing the transition from cold to temperate firn on Austfonna ice cap, Svalbard, through observations and model simulations

Satu Innanen[1], Regine Hock[1,2], Louise Steffensen Schmidt[1], Thomas V. Schuler[1], Federico Covi[1,3] and Geir Moholdt[4]

[1]Department of Geosciences, University of Oslo, Oslo, Norway; [2]Geophysical Institute, University of Alaska Fairbanks, Fairbanks, AK, USA; [3]British Antarctic Survey, Cambridge, United Kingdom and [4]Norwegian Polar Institute, Fram Centre, Tromsø, Norway

Article

Cite this article: Innanen S, Hock R, Schmidt LS, Schuler TV, Covi F, Moholdt G (2025) Witnessing the transition from cold to temperate firn on Austfonna ice cap, Svalbard, through observations and model simulations. *Journal of Glaciology* **71**, e101, 1–13. https://doi.org/10.1017/jog.2025.10072

Received: 31 December 2024
Revised: 1 June 2025
Accepted: 7 July 2025

Keywords:
firn; firn cores; ice cap; refreezing; Svalbard

Corresponding author: Satu Innanen;
Email: s.k.innanen@geo.uio.no

Abstract

Refreezing is a critical component of the mass balance of glaciers in Svalbard, yet the processes and changes under a warming climate are not fully understood. Here, we investigate changes in firn properties of the Austfonna ice cap, Svalbard, using a combination of observations and model simulations. We analyze firn stratigraphy and density from five newly retrieved and 11 previously retrieved firn cores, collected at elevations ranging from 506 m a.s.l. to 791 m a.s.l. between 1958 and 2022. All cores exhibit frequent ice layers that indicate persistent refreezing of meltwater; however, no ice slabs (layers exceeding 1 m) were observed. A 13-year-long firn temperature time series from a site near the summit (773 m a.s.l.) shows that annual water percolation reaches depths of 7 m to over 13 m. A notable transition in the firn thermal regime occurred in 2013, transitioning from cold to temperate conditions above the firn-ice interface despite the seasonal cooling occurring in the upper firn layers. Simulations using the CryoGrid community model from 2009 to 2022 corroborate this thermal shift and suggest the development of a firn aquifer multiple times since 2013, with increasing duration and thickness over time.

1. Introduction

Svalbard is one of the fastest warming regions on Earth (Nordli and others, 2014; Isaksen and others, 2016). Glaciers, which cover 57% of the archipelago (Nuth and others, 2013), are significantly impacted by increasing surface melt due to rising temperatures. During 2000–19, Svalbard glaciers lost mass at a rate of -8 ± 6 Gt a^{-1} (Schuler and others, 2020), and mass loss is projected to increase in the coming decades (Hock and others, 2019; van Pelt and others, 2021; Geyman and others, 2022).

The impact of increasing melt rates on total mass loss and associated sea level rise depends on the amount of water that runs off from the glacial system. Here, firn plays an important role by retaining meltwater and reducing runoff in the accumulation zones (Pfeffer and others, 1991; Harper and others, 2012). In Svalbard glaciers, refreezing is a significant component of the climatic mass balance – the sum of the surface and internal mass balance (Cogley and others, 2011) – accounting for around 25% of the annual accumulation (Aas and others, 2016; Østby and others, 2017; van Pelt and others, 2019; Schuler and others, 2020). However, the reduction in firn cover extent and concomitant firn densification have led to a decrease in firn pore space in Svalbard glaciers, thereby diminishing their firn buffering capacity (Østby and others, 2017; van Pelt and others, 2019; Noël and others, 2020). This negative trend is projected to continue during the 21st century (van Pelt and others, 2021).

Numerous studies have reported a drastic reduction in firn retention capacity in some polar regions due to the formation of ice slabs ($>$ 1 m thick ice layers) near the surface, which prevent meltwater flow to greater depths (Machguth and others, 2016; MacFerrin and others, 2019). Ice slabs have been discovered in the western and northern Greenland (MacFerrin and others, 2019), and in the Canadian Arctic (Bezeau and others, 2013). Furthermore, firn aquifers, liquid water reservoirs in firn pore space that do not refreeze over winter (Forster and others, 2014), have been detected along the southeastern margin and northwest of Greenland (Forster and others, 2014; Miège and others, 2016), in central (van den Akker and others, 2025) and northwestern Svalbard (Christianson and others, 2015), and in Antarctica (Montgomery and others, 2020). In the past two decades, an expansion of both ice slabs and firn aquifers has been observed on the Greenland Ice Sheet (Horlings and others, 2022; Jullien and others, 2023). The presence of ice slabs or firn aquifers predominantly depends on the rates of surface water input (melt and rain) and snow accumulation (Brils and others, 2024).

How the stratigraphic and thermal properties of firn will change in the warming climate is a question of high importance due to the impact on meltwater retention capacity, glacier hydrology, and dynamics. By sealing off pore space, ice slabs can increase runoff and accelerate mass loss (Machguth and others, 2016; MacFerrin and others, 2019), while perennial firn aquifers can delay runoff (Forster and others, 2014). Moreover, ice velocity may be largely affected by water potentially draining from aquifers to the glacier bed through crevasses (Poinar and others, 2017; Cicero and others, 2023), and by liquid water storage in firn altering the thermal regime of the ice (Irvine-Fynn and others, 2011; Wilson and Flowers, 2013).

Previous observational studies on long-term changes in firn properties have largely focused on Greenland and the Canadian Arctic. This work extends those studies to Svalbard by focusing on Austfonna – an Arctic ice cap where changes in firn due to recent atmospheric warming have not yet been documented. We combine field observations and modeling to gain a better understanding of the stratigraphy and thermal state of the firn, as well as the meltwater retention processes on the ice cap. We present data from 16 firn cores drilled on Austfonna between 1958 and 2022, exploring spatial and temporal changes in density and ice content. Additionally, we provide a firn temperature record spanning from 2009 to 2022. Furthermore, we apply the CryoGrid community energy balance model to simulate changes in firn temperature, water content, and density. In situ surface mass balance, temperature, and density data are used to validate the model. The results are relevant to other glaciers and ice caps in the Arctic, as the rapid warming in Svalbard may signal broader changes that could affect other regions in a similar way.

2. Study area

Austfonna is located on Nordaustlandet in northeastern Svalbard, centered at 79.7 °N and 24 °E (Fig. 1). With an area of $> 7800\,km^2$ (Moholdt and Kääb, 2012), Austfonna is the largest ice cap in the Svalbard archipelago, accounting for a third of its ice volume (Fürst and others, 2018). The ice cap ranges in elevation from sea level up to around 800 m above sea level (a.s.l.), where the thickest ice of about 500 m is found (Dowdeswell and others, 1986). Three of the marine-terminating basins have been observed to surge in the past (Lefauconnier and Hagen, 1991), and two ongoing surges have been occurring in Basin-3 and Etonbreen since 2012 and 2023, respectively (Dunse and others, 2015; Mannerfelt and others, 2025).

The mean annual air temperature measured at a weather station on Austfonna at 370 m a.s.l. over the period 2004–12 was −8.3°C, with hourly values ranging from −43.2°C to 9.1°C (Schuler and others, 2014). Temporal variability is high; even in winter, the temperature can occasionally rise to above 0°C, while summer snowfalls may also occur. The melt season typically lasts from mid-June to the end of August or beginning of September (Schuler and others, 2007, 2014). The primary moisture source for Austfonna's precipitation is the Barents Sea east-southeast of Svalbard (Pinglot and others, 2001; Taurisano and others, 2007).

Surface mass balance measurements using the glaciological method are available for Etonbreen, a 640 km^2 glacier draining the ice cap to the west. From the mass balance years 2003/04 to 2021/22, the winter balance was 0.40 m w.e. and the summer balance was −0.54 m w.e. resulting in an annual balance of −0.14 m w.e. (Fig. 2). While the winter balance is relatively stable, the summer balance, and consequently also the annual balance, vary considerably from year to year. Particularly high melt occurred in the summers of 2004, 2013, 2020 and 2022 with annual mass balances of −0.56 m w.e., −0.59 m w.e., −0.76 m w.e. and −0.82 m w.e., respectively. The equilibrium line altitude (ELA) of Etonbreen was in average 556 m a.s.l. in 2004–22 (Fig. 2). Accumulation rates are generally higher in the southeast of the ice cap compared to the northwest, as shown by observations from shallow ice cores (Pinglot and others, 2001) and ground-penetrating radar (GPR) (Taurisano and others, 2007; Dunse and others, 2009). This is consistent with the primary moisture source originating from the Barents Sea. Mapped glacier facies based on GPR measurements indicate that even the summit area has been subject to melting during the summer, with no dry snow zone present (Dunse and others, 2009). Superimposed ice is typically found in the lower accumulation area.

3. Data and methods

3.1. Firn cores

We use data from five new firn cores retrieved in 2022 and 11 earlier cores from various sources (Table 1) and locations (Fig. 1). To identify where and when each core was drilled, the following nomenclature is used: site_year, where "site" refers to the location and "year" to the core retrieval year.

3.1.1. Firn cores drilled in 2022

Between 11 and 16 May 2022, a total of five shallow firn cores were collected at Etonbreen. Four cores (Eton-4_22, Eton-5_22, Eton-6_22 and Camp_22) were retrieved along the mass balance stake transect, with one core (RR-3_22) being retrieved slightly outside of it. The cores were extracted using a KOVACS Mark III ice coring system, which consists of a 1 m core barrel with a diameter of 7.25 cm, extension rods, and an adapter for an electric drill machine. Cores RR-3_22 and Eton-5_22 were collected from the snow surface, while the three other cores were collected from the snow-firn interface of a snowpit.

The drilling procedure and measurement techniques closely followed the methods of Rennermalm and others (2022). After each core section was extracted, its length was measured, and it was photographed in a half-pipe against an aligned ruler. Core section lengths varied substantially (0.32 ± 0.22 m, mean ± standard deviation). Sections often broke naturally into smaller pieces or were cut manually so that their lengths varied roughly between $0.1 - 0.2$ m. These shorter pieces (hereinafter called segments following Rennermalm and others (2022)) were weighed using an OHAUS CS Series scale (capacity 2000 g, accuracy 1 g), and their length and diameter were measured with a stiff measuring tape and a caliper, respectively. Additionally, the segment intactness (in percent) was visually estimated, as segments were often not complete (e.g., some material was lost at the edges). The thickness and depth of ice layers were logged with a resolution of 0.005 m and thinner ice layers were recorded with a thickness of 0.0025 m. Coring became more challenging when approaching the glacier ice, as the barrel tended to get stuck and thus, the total lengths of the cores vary considerably ($2.8 - 9.7$ m). We refer to glacier ice as ice that we assume is not underlain by firn, which distinguishes it from an ice layer.

We calculate the density of each core segment from the measurements of diameter, length, weight, and intactness. Density for 15% of core segments exceeded the density of pure ice (917 kg m^{-3}) and was corrected as described in the Supplementary Text. The mean density (± standard deviation) of all pure ice segments $853 \pm 52\,kg\,m^{-3}$ is consistent with previous studies

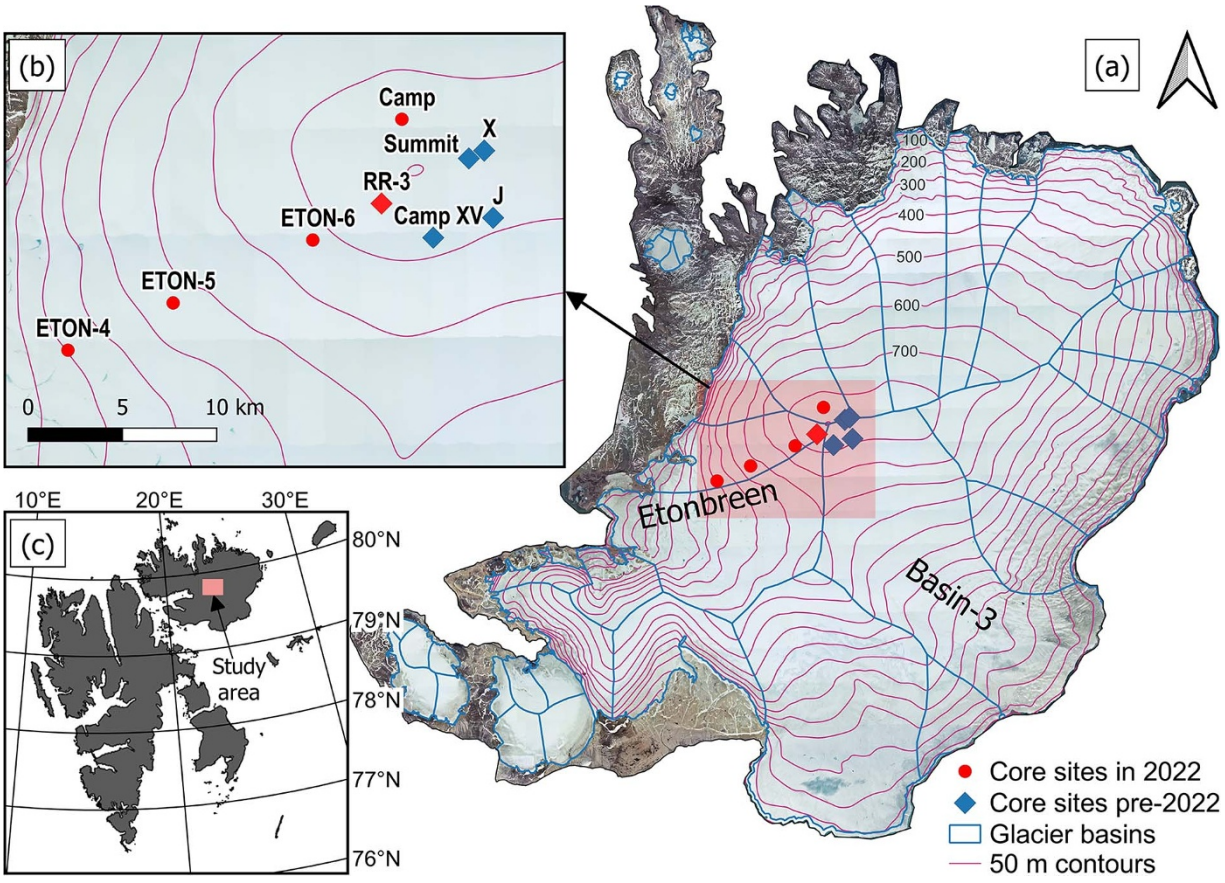

Figure 1. (a) Study area Austfonna ice cap, (b) sites of newly and previously drilled firn cores presented in this study, and (c) location on the Svalbard archipelago. 50 m contour lines and glacier basins are derived from a digital elevation model (DEM) based on aerial photos from 2011 (Norwegian Polar Institute, 2014b). Elevation contours are in m a.s.l.. The basemap is derived from an orthophoto from 2012 (Norwegian Polar Institute, 2014a).

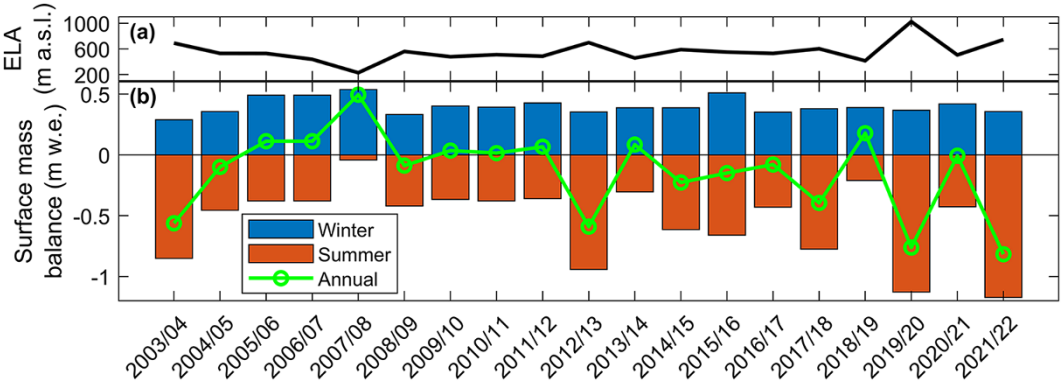

Figure 2. (a) Equilibrium-line altitude (ELA) and (b) annual, winter, and summer glacier-wide surface mass balance of Etonbreen derived from stake and snow pit measurements for the mass-balance years 2003/04 to 2021/22. Note that the ELA is derived from the mass-balance gradient and therefore exceeds the maximum elevation of the ice cap in 2019/20.

that found ice densities ranging from 843 ± 36 kg m^{-3} to 873 ± 25 kg m^{-3} (Harper and others, 2012; Machguth and others, 2016; Rennermalm and others, 2022).

3.1.2. Previously drilled cores

We used data from 11 cores collected near the summit area between 1958 and 2015 (Table 1). Four cores were drilled between 2004 and 2015 by the University of Oslo and the Norwegian Polar Institute using similar methods as described above. Data from seven cores have previously been published (Table 1). One of them was drilled at Camp XV in 1958 (Schytt, 1964), two at site J in 1998 and 1999 (Watanabe and others, 2001), two at site X in 1999 (Pinglot and others, 2001) and 2010 (Langhammer, 2014), and two at Summit in 2012 and 2013 (Langhammer, 2014). Among the various cores presented by Pinglot and others (2001), we use only core X_99 due to its proximity to the summit area and its comparable elevation to the other drill sites.

The density data of all cores were corrected where necessary (Supplementary Text). Some earlier cores were drilled from the snow surface, and the depth of the snow-firn interface had to be

Table 1. Firn cores used in this study. The last number in the core name refers to the core retrieval year. The elevations are taken from the original source, or, if not available, derived from the DEM by Norwegian Polar Institute (2014b). The drilling depth refers to the depth below the snow surface. The segment length is the length over which density was measured. The sources refer to (1) this study, (2) Langhammer (2014), (3) Watanabe and others (2001), (4) Schytt (1964), and (5) Pinglot and others (2001).

Core	Year	Date	Elevation (m a.s.l.)	Elevation source	Drilling depth (m)	Segment length mean ± std dev. (m)	Source
Eton-4_22	2022	15 May	506	DEM	3.9	0.15 ± 0.06	1
Eton-5_22	2022	16 May	637	DEM	4.3	0.17 ± 0.15	1
Eton-6_22	2022	11 May	736	DEM	7.3	0.14 ± 0.04	1
Camp_22	2022	13 May	773	DEM	10.2	0.13 ± 0.05	1
RR-3_22	2022	15 May	784	DEM	10.7	0.14 ± 0.11	1
RR-3_15	2015	6 May	784	DEM	13.4	0.37 ± 0.13	1
RR-3_14	2014	5 May	784	DEM	10.2	0.42 ± 0.14	1
Summit_13	2013	5 May	791	DEM	16.3	0.32 ± 0.21	2
Summit_12	2012	5 May	791	DEM	10.3	0.25 ± 0.11	2
X_10	2010	25 April	782	DEM	10.0		2
X_08	2008	23 April	782	DEM	7.6	0.54 ± 0.17	1
J_04	2004	April	765	DEM	16.4	0.18 ± 0.07	1
X_99	1999	April–May	783	Source	11.1	0.28 ± 0.11	5
J_99	1999	April–May	750	Source	289.0	0.54 ± 0.25	3
J_98	1998	19 March – 3 April	750	Source	119.0	0.55 ± 0.19	3
CampXV_58	1958	21 June	765	Source	6.8	0.13 ± 0.04	4

estimated. This was done based on snow pit measurements from the same year or by scrutinizing density profiles (typically a clear spike in density was found below the snow-firn interface).

3.2. Firn temperature

Firn temperatures have been monitored near the summit at site Camp (Fig. 1) by the University of Oslo and the Norwegian Polar Institute since 2009. A thermistor string with 10 temperature sensors was inserted into a borehole on 6 May 2009, which was then backfilled with snow. The sensors were spaced at intervals of 1 to 3 m, with the lowest sensor located at 13 m below the snow surface. Data were recorded until 29 April 2014. A second thermistor string was installed, and logging started on 3 May 2014, with the lowest sensor positioned at a depth of 12 m. An 8-month gap from August 2018 to April 2019 occurred due to full memory of the storage unit. A third thermistor string was installed on 3 May 2015 logging data until 2022. The lowest sensor was located at a depth of 11.2 m at installation.

Since continuous surface height measurements at site Camp are not available, we used surface heights simulated by the CryoGrid community model (Schmidt and others, 2023; Westermann and others, 2023) (described in the next section) to track the temporal evolution of sensor depths. For all three thermistor strings, the sensor depths were initialized from the depths recorded at installation. We did not account for movement of the sensors due to firn compaction when assessing sensor depths over time.

We corrected the sensor readings for systematic biases by shifting each thermistor string's time series by the observed bias at 0°C, by using temperature measurements during melting conditions. The average bias for the three thermistor strings was 0.25°C, −0.10°C, and −0.16°C, respectively. Data from the first two months after the installation of each thermistor were discarded to ensure records were not affected by disturbances from the drilling procedure.

3.3. Modeling

3.3.1. Model description

To simulate subsurface firn temperature, density, and water content at site Camp, we used the multi-layer, energy balance model CryoGrid (Westermann and others, 2023). While originally developed for permafrost, it has recently been adjusted for glacier applications (Schmidt and others, 2023). Our model set-up closely follows Schmidt and others (2023). Below, we present a brief description of the model while further details and model parameter values used in this study are given in the Supplementary Text and Supplementary Tables S1-S3.

The model calculates the energy flux toward the surface from the surface energy balance. When the surface temperature is below the melting point, the excess energy is used to remove the cold content. Once the surface becomes temperate, excess energy is used for melting. The subsurface scheme accounts for snow and firn compaction, heat transport, refreezing, water percolation, and runoff. The parameterizations of subsurface processes are based on the snowpack model Crocus (Vionnet and others, 2012), with a few modifications.

CryoGrid uses the so-called tipping bucket approach (Westermann and others, 2023) to simulate the water balance; water infiltrates by gravity to the next, underlying layer, when the field capacity (0.05 m^3 m^{-3}) of the current layer is exceeded.

Runoff may occur in layers above an impermeable layer (defined by density > 830 kg m^{-3}) if the amount of water surpasses the field capacity (Westermann and others, 2023). Runoff is delayed by a runoff time scale, allowing water to be stored in a layer until it refreezes or runs off. In contrast to previous applications, here some water is allowed to flow through individual "impermeable" layers if they overlay permeable firn. The amount of water depends on the hydraulic conductivity of the layer above it, which is influenced by the snow grain diameter, snow density, and saturation (see Schmidt and others (2023)). This modification was necessary to prevent pooling of water near the surface, as this was not supported by observations. Water input to the surface layer originates from snow/firn melt or rainfall. Lateral water movement is not considered.

Calculations are performed on a vertical grid with user-prescribed initial vertical spacing. Here, the top layer was assigned a thickness of 0.01 m w.e., and layer thickness doubles every 20 layers. Snow and firn layers are merged or split using a layer thickness criterion (Zweigel and others, 2021; Schmidt and others, 2023): when the layer exceeds the user-defined snow water equivalent

threshold by more than 50%, it is divided in half. A layer is merged with the underlying one, when the current layer is 50% below the threshold. Hence, the surface snow or firn layer thickness ranges from 0.005 m w.e. to 0.015 m w.e.. Below the firn-ice interface, we used 38 ice layers with a total thickness of 30 m, which remain constant throughout the simulation period.

The model was forced by 2 m air temperature, wind speed, specific humidity, incoming shortwave and longwave radiation, precipitation, and air pressure from the Copernicus Arctic Regional ReAnalysis (CARRA) (Schyberg and others, 2020). The temporal resolution is 3 hours, and the spatial resolution is 2.5 km. We use the grid point closest to site Camp's elevation.

3.3.2. Model initialization and application

The model was run over the period from 1 January 2009 to 31 December 2022 to encompass the entire period of firn temperature observations. Since thermistor measurements were not available before May 2009, we used the data from 1 January 2010 to represent the thermal conditions at the start of the simulation (Supplementary Table S3). Firn density was initialized with firn core observations from Summit_2012, as this is the firn core closest in time to our simulation start date and has a long enough density record. Both temperature and density observations were linearly interpolated to the model layers. In the absence of direct observations of the depth of the firn-ice interface at site Camp in 2009, we assumed a depth of 10 m, based on available observations nearby (Core X_10, GPR measurements from Dunse and others 2013, and average seasonal snow depth (Dunse and others, 2009)).

4. Results

4.1. Firn density and stratigraphy

Figure 3 illustrates the stratigraphy and density profiles of the five new cores drilled in May 2022. Core Eton-4_22 (506 m a.s.l.) and core Eton-5_22 (637 m a.s.l.) are located slightly below and above the average ELA for the period 2004–22 (556 m a.s.l.), respectively. Therefore, we assume that glacier ice is found at depths of −1.3 m and −3.1 m in Eton-4_22 and Eton-5_22, respectively. However, for cores Eton-6_22, Camp_22, and RR-3_22, the depth of the firn-ice interface is less clear; we assume the bottom layers to be ice layers rather than part of the continuous ice body underlying the firn. All cores display numerous ice layers throughout their entire length. The thickest ice layer was found at Eton-6_22 and was at least 0.79 m thick. Firn thickness varies substantially with elevation, increasing from 0.12 m (Eton-4_22) to >10 m at the highest core (RR-3_22) 18 km away. Density and ice content increase with depth (Fig. S1). While density and ice content are higher in the first few meters at Eton-5_22, there is no discernible decreasing trend with increasing elevation among the three highest cores (736 — 784 m a.s.l.) (Fig. S1).

Figure 4 shows the firn stratigraphy and density of the 13 cores drilled in close proximity to the summit between 1958 and 2022 (Fig. 1). The drilling sites are up to 7 km apart from each other, but the elevation differences between them are <41 m and thus, spatial variations in climatic conditions can be assumed small. The thickest ice layer among these cores is found in core J_99 (0.81 m located below −6 m depth). The depth of the firn-glacier ice transition varies among the cores and over time. At site J, this depth was −8.3 m in 1998, −8.7 m in 1999, and −6.8 m in 2004. Core J in 2004 displays the shallowest firn column among all cores, while the deepest firn column is found at Summit in 2013 (12.3 m). Despite spanning more than 60 years, the cores drilled in the summit area show no apparent trend in the abundance or distribution of ice layers.

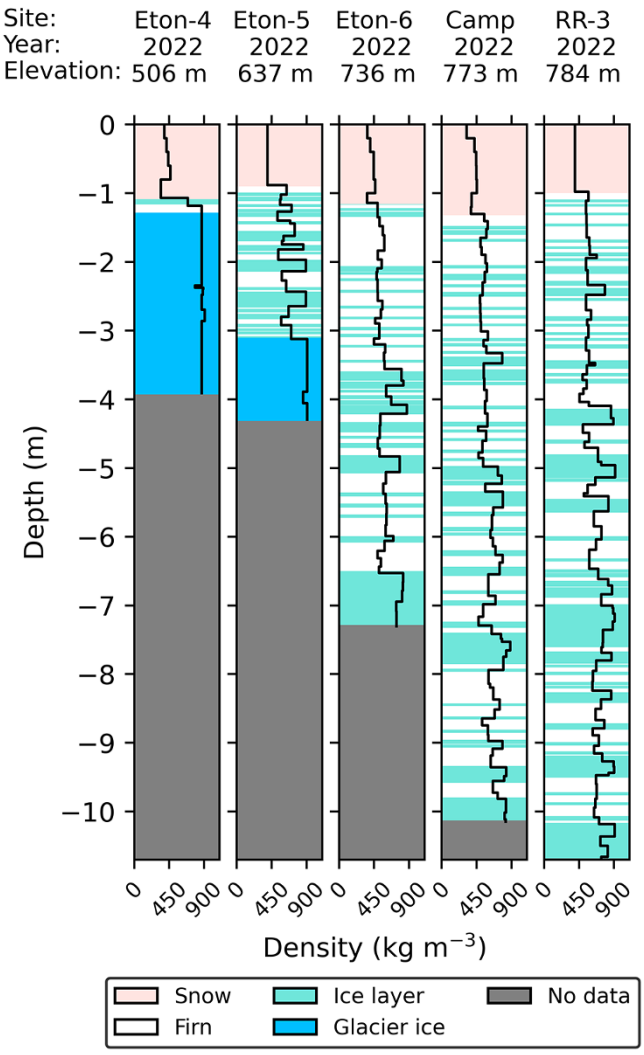

Figure 3. Firn stratigraphy and density for cores drilled on Austfonna in May 2022 in order of ascending elevation from left to right (sites in Figure 1). Elevations are in m a.s.l. from the DEM by Norwegian Polar Institute (2014b). Black lines show the density for each segment.

4.2. Firn temperature

Measured subsurface temperatures at site Camp from May 2009 to December 2022 show seasonal variations between winter cooling and summer melt (Fig. 5a). However, what stands out is a clear transition in the firn thermal state. Between 2009 and 2013, firn is seasonally temperate during summer and fall, warmed by meltwater percolation and refreezing, while temperatures otherwise remain below 0°C. No temperate firn persists throughout the entire year, suggesting that all meltwater refreezes in the subsequent winters. However, after 2015, firn becomes temperate year-round at depth, with sub-freezing temperatures found only near the surface during winter. This thermal regime shift occurred between 2013 and 2015, although precise timing is unclear due to data gaps and the temperature sensors not reaching sufficient depth. Field observations in May 2014 at sites Camp and RR-3 support the presence of liquid water (and temperate firn): liquid water was encountered in the lower part of the borehole at Camp during the installation

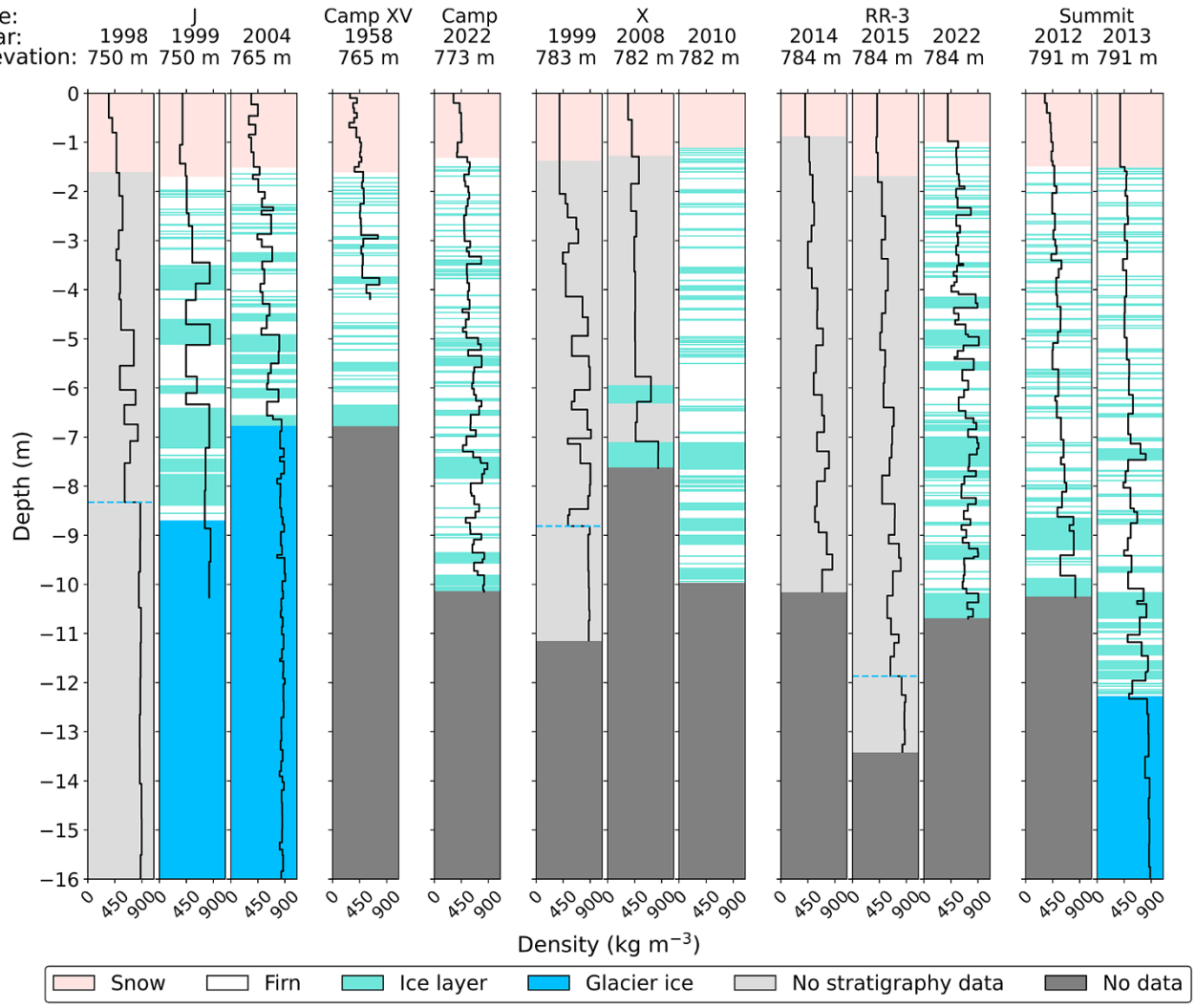

Figure 4. Firn stratigraphy and density for cores drilled in the summit area (sites in Figure 1) between 1958 and 2022. Elevations are in m a.s.l from the DEM by Norwegian Polar Institute (2014b) or from the original sources (Table 1) ranging from 750 m a.s.l. to 791 m a.s.l.. Black lines show the mean density for each core segment. Only the upper 16 m is shown for cores that are longer. Dashed blue line indicates the start of glacier ice for cores with no stratigraphy data based on densities and/or other field observations.

of a new thermistor string, and at −10.2 m depth when drilling a firn core at RR-3. Based on the temperature record and field observations from the pre-melt season in 2014, we infer that the shift to year-round temperate firn at depth likely occurred in 2013.

Meltwater percolation depth, inferred from temperatures ≥ -0.1°C, increased between 2009 and 2013 (Fig. 5a). In summer 2009, meltwater percolated down to approximately 7 m below the surface, while by summer 2013, it reached depths exceeding 10 m below the surface. After the shift to temperate conditions at depth in 2013, meltwater percolated considerably deeper, reaching at least 13 m below the surface by the end of the record. Interestingly, between 2009 and 2013, meltwater did not percolate below a depth of approximately 8 m below the May 2009 surface. This indicates either an ice layer or glacier ice blocking the percolation.

4.3. Model validation

The model was validated by comparing the simulation results with observations of surface mass balance, firn temperature, and firn density. The observed and modeled cumulative surface mass balance over the mass-balance years 2009/10 to 2018/19 align well (Fig. 6).

The simulated subsurface temperature closely follows the measurements. The correlation coefficient between daily modeled and observed temperatures is 0.70, and the root mean square error is 2.6°C (Fig. 5c). Except when the firn is temperate, the simulated temperature profile is colder with a mean difference between the simulated and observed temperature of −1.2°C. Especially from summer 2010 to spring 2013, the simulated firn is notably colder and meltwater percolation is shallower than observed (Fig. 5a,b). For example, in summer 2010, meltwater percolates to 7.5 m below the surface, whereas the simulated percolation reaches 2 m below the surface. After summer 2013, both the simulation and observations generally indicate temperate conditions at depth, with temperature differences concentrated near the surface. In some years, such as winters 2010 and 2016, the simulated firn is too warm, with differences of up to 2°C (Fig. 5c).

Simulated and observed densities in six firn cores drilled in the summit area of Austfonna generally match well, despite small-scale

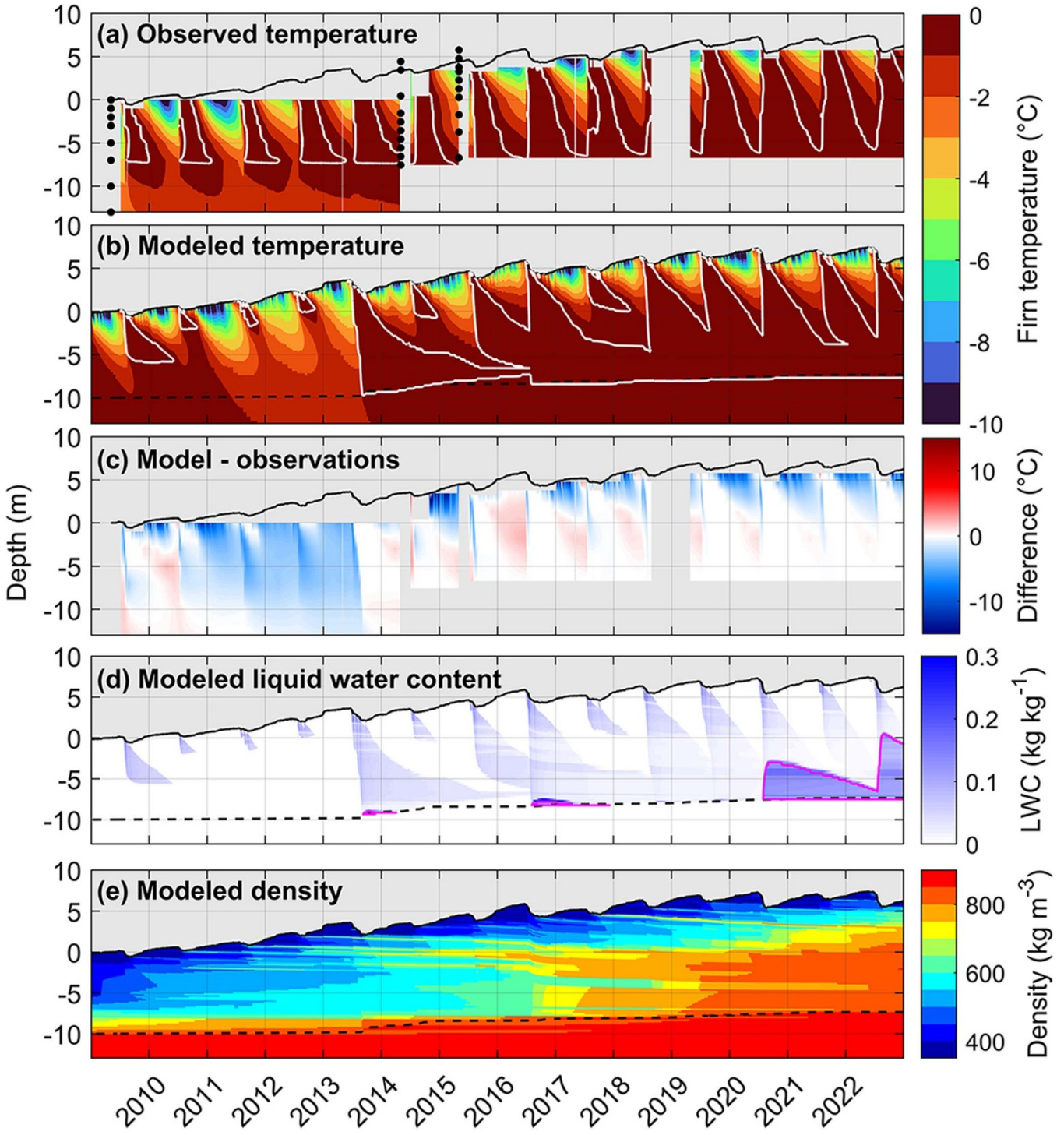

Figure 5. (a) Observed and (b) modeled firn temperatures at site Camp, and (c) their differences, (d) modeled liquid water content (LWC) and (e) density from 2009 to 2022. The black solid line indicates the surface as derived from the simulation, and the dashed line shows the modeled firn-glacier ice interface (derived from density $\geq$ 830 kg m^{-3} with no permeable layers below). The depth is relative to the surface on 6 May 2009. The black dots in (a) show the temperature sensor locations at installation. The white line outlines the presence of liquid water which is inferred from temperatures $\geq -0.1^{\circ}$C (panel a) and liquid water content $\geq$ 0.001 kg kg^{-1} (panel b). The pink line in (d) outlines fully saturated firn (saturation $\geq$ 99%).

discrepancies due to stratigraphic features such as ice layers (Fig. 7). For three cores, we find negative model biases of −2 kg m^{-3} (RR3_15), −22 kg m^{-3} (Summit_12) and −44 kg m^{-3} (RR3_14). For three other cores, we find positive model biases of 4 kg m^{-3} (Summit_13), 29 kg m^{-3} (RR3_22), and 74 kg m^{-3} (Camp_22). In core Camp_22, where the model overestimates density the most, the largest difference occurs below −4 m depth. Overall, the model validation provides confidence in the model's performance, despite some shortcomings in accurately predicting firn temperature and density.

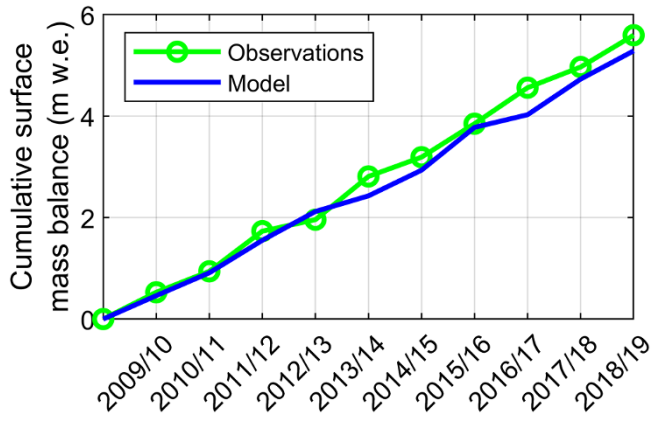

Figure 6. Cumulative surface mass balance derived from stake and snow pit measurements at site Summit and simulated for site Camp for the balance years 2009/10 to 2018/19. The model assumes that the start of the mass-balance year is 1 September.

4.4. Simulated firn conditions

Modeled firn temperature and liquid water content indicate that between 2009 and 2013, the firn is seasonally temperate, with summer melt percolating to depths of 1.7−5.0 m below the surface (Fig. 5b,d). However, in 2013, meltwater is simulated to percolate down to 13.5 m below surface, resulting in some firn to remain temperate throughout the year as winter cold temperatures no longer penetrate the entire firn column. In the summers of 2014 and 2017, simulated meltwater does not reach deeper than approximately 3−5 m below the surface, but temperate firn is preserved below ∼ 10 m from the surface.

According to the simulation results, seasonal aquifers form in 2013, 2016-17 and 2020-22, when water pools above the glacier ice, and the firn is saturated. In the summers of 2020 and 2022, the top of the saturated firn is shallowest at 8 m and 5 m below the surface, respectively. The depth of the water table is highest in summer and decreases toward winter.

Densities range from 298 kg m^{-3} to 917 kg m^{-3}, increasing with depth (Fig. 5e). The annual mean density averaged over the top 10 m increases significantly between 2009 and 2022 (p-value < 0.01), rising from 524 kg m^{-3} to 711 kg m^{-3}.

Cold content peaks in 2011, followed by a subsequent decline; however, no statistically significant trend is observed (Fig. 8a). The year 2011 is the coldest in the simulation, with a mean annual temperature of −5.7°C in the top 10 m, and the firn column is cold throughout below the summer melt. Cold content reaches a minimum in 2016, which is the warmest year in the simulation, with a mean annual temperature of −1.8°C in the top 10 m, associated with temperate conditions below the penetration depth of seasonal cold.

The highest annual amounts of refreezing in the top 10 m occur in 2013 and 2017, with values of 0.48 m w.e., and 0.42 m w.e., respectively (Fig. 8b). However, no statistically significant trend is detected. Sharp increases in refreezing are related to more available meltwater. In contrast, simulated pore space decreases significantly (p-value < 0.01) during this period (Fig. 8c). The decrease in pore space is connected to increases in density within the same period (Fig. 5e).

5. Discussion

5.1. Temporal changes in firn density and stratigraphy

To investigate temporal changes in firn stratigraphy, we examine variations in average density and ice content across three sections (0–3 m, 3–6 m and 6–9 m from the surface) among all available firn cores near the summit (Fig. 9). No clear temporal trends can be detected. However, in all sections, density appears lower between 2008 and 2015 compared to before and after, with ice content in the middle sections following this pattern. Core J_99 exhibits exceptionally high ice content in the bottom section, reaching 62%. Comparing cores drilled over the years by various field teams is challenging due to the lack of international standardized measurement protocols for retrieving and measuring firn core properties. Additionally, ice content and density can vary considerably on small scales (within meters) (Marchenko and others, 2017a; Xiao and others, 2022), which may impact the representativeness of a single core from a given year. Nevertheless, we find that our observed variations in firn stratigraphy are consistent with variations in melt.

To explore mechanisms behind the observed and simulated variations in firn properties, we calculate annual positive degree day (PDD) sums, defined as the sum of mean daily air temperatures above the melting point (Cogley and others, 2011), as a proxy for melt (Fig. 10). We use the CARRA dataset for site Camp from 1993 to 2022, which is the same dataset used to force the model simulations. The mean PDD sum over this 30-year period is 37 K d. Between 2005 and 2012, the PDD sum is approximately at or below average, ranging from 7 to 39 K d, indicating an 8-year period with little melt. From 2013 onward, several years – such as 2013, 2015, 2020 and 2022 – exhibit PDD sums substantially higher than the 30-year average.

We find significant correlations between firn core density in the middle (3-6 m) and bottom (6-9 m) sections and the PDD sum of the year preceding core retrieval (p-values < 0.01, Fig. 11). This indicates deep meltwater percolation and refreezing, which is further supported by the temperature data. Intensive melt years lead to decreased pore space; conversely, the period of approximately average or below average melt from 2005 to 2012 may have caused the decrease in firn density and ice content in cores collected from 2008 to 2013 compared to those from 1998 to 2004. This indicates that firn pore space can replenish when less meltwater infiltrates and refreezes in the firn. The increased density in 2022 may be related to the high melt year of 2020. Our findings that firn density is affected by changes in annual melt are consistent with firn core studies from other regions (e.g. Braithwaite and others, 1994; Bezeau and others, 2013; Machguth and others, 2016; Rennermalm and others, 2022). To explore the longer-term impact of melt on firn density, we also correlate density for each section with mean PDD sums from two to five years prior to core retrieval (Fig. S2). Results suggest that for the middle section, melt conditions up to three years prior to core retrieval also affect the evolution of the stratigraphy. However, further data are needed to confirm these findings.

Our examination of the firn stratigraphy reveals an absence of ice slabs (> 1 m ice layers) in the summit area of Austfonna, in contrast to recent observations from Greenland (e.g. Machguth and others, 2016; MacFerrin and others, 2019; Rennermalm and others, 2022) and the Canadian Arctic (e.g. Zdanowicz and others, 2012; Bezeau and others, 2013; Gascon and others, 2013). In Greenland, ice slabs have expanded and thickened since 2000 (MacFerrin and others, 2019; Jullien and others, 2023), and they have been shown

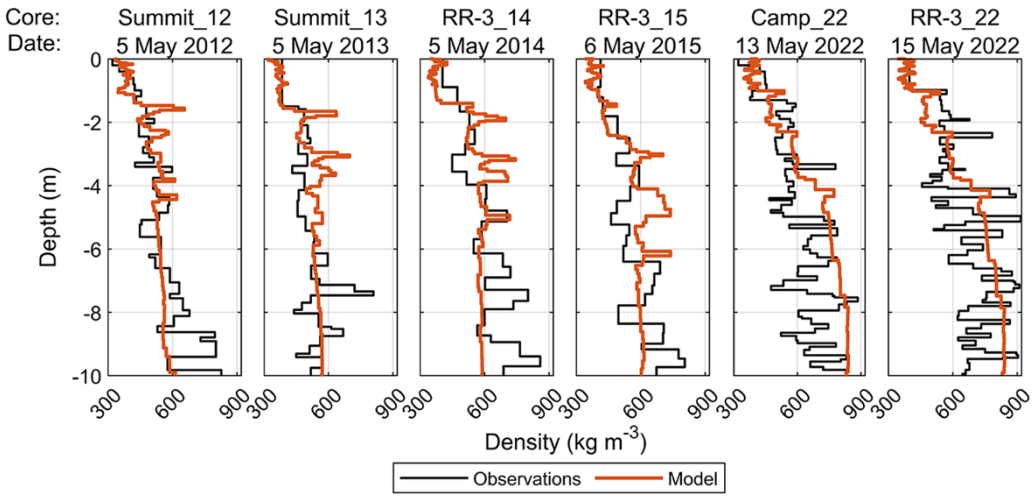

Figure 7. Observed and simulated density in the upper 10 m of six cores drilled in the summit area between 2012 and 2022. Observed and simulated densities refer to averages over each measured segment and each simulated layer thickness, respectively.

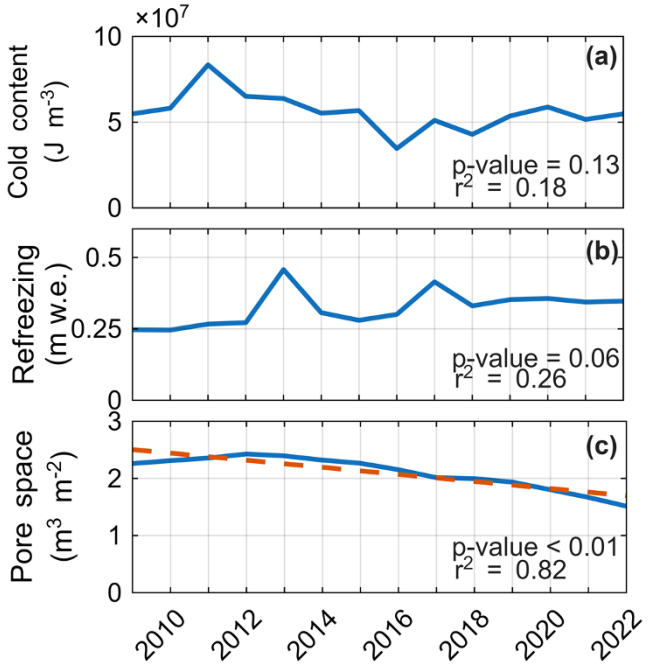

Figure 8. Modeled annual (a) cold content, (b) refreezing, and (c) firn pore space in the top 10 m from 2009 to 2022. Annual values are derived from averaging (a, c) and summing (b) daily model output. The dashed line is the linear fit (only shown when significant; p-value < 0.05). The p-value is the probability value at a 95% confidence level, and r^2 is the coefficient of determination.

to form rapidly after an extreme melt season (Culberg and others, 2021). Here, even extreme melt years like 2020 (Figs. 2, 10) do not considerably alter the firn stratigraphy so that thick impermeable layers form. Hence, the effect of ice slabs in accelerating runoff and mass loss by limiting percolation has likely not been relevant at our sites.

5.2. Firn thermal regime

Our firn temperature observations and modeling results indicate that between 2009 and 2022, the thermal regime of the firn at depth shifted from cold to temperate conditions throughout the year. Both observations and model simulations indicate that this thermal transition most likely occurred in 2013, suggesting that a single extreme melt year can induce a lasting change in the firn thermal regime. We note that in some years, simulated meltwater percolation is considerably shallower than the observed depths, and subsurface temperatures generally have a cold bias (Fig. 5c). The absence of a parameterization for deep percolation due to preferential flow paths in firn (Marchenko and others, 2017b) could at least partially account for the observed cold bias below the wetting front. Nevertheless, the model captures the observed regime shift, indicating that this shift is a robust feature.

Similar shifts in the thermal state of deeper firn, transitioning from cold to temperate year-round, have been inferred based on temperature measurements in central Svalbard comparing data from 1965 and 1976 to data from 2012 and 2013 (Marchenko and others, 2017a), as well as through simulations covering period 1957–2014 (Østby and others, 2017). However, our study is the first in Svalbard to document a thermal shift based on continuous multi-year observations further supported by firn modeling.

Firn temperature observations in the summit area of Austfonna are scarce before 2009. Schytt (1964) reported a temperature of −4.2°C at a depth of 7 m below the surface at Camp XV in 1958. Watanabe and others (2001) found firn temperatures of −1°C and −2.8°C at −10 m depth at site J in 1998 and 1999, respectively. Zagorodnov and others (1989) observed predominantly negative temperature profiles in 1987; however, in two boreholes, temperatures increased with depth, approaching the melting point at approximately 6−7 m below the surface.

5.3. Firn aquifer

The model simulations indicate that, following the shift in thermal regime, firn aquifers formed above the simulated firn-ice interface in 2013, 2016-17 and 2020-22. We attribute the aquifer formation to year-round temperate firn and deep meltwater percolation, the latter facilitated by the absence of ice slabs. The aquifer appears

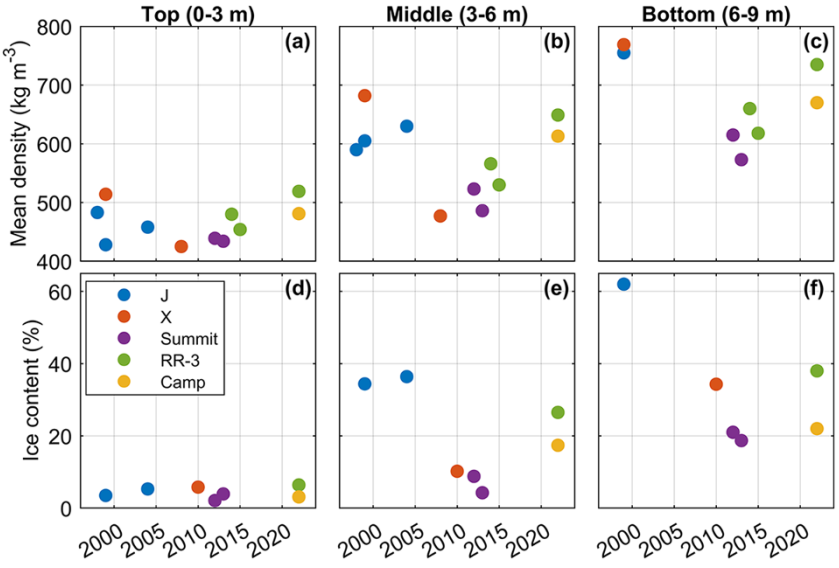

Figure 9. Mean density (a-c) and ice content (d-f) from 1998 to 2022 for the top (0-3 m, 11 and 7 cores for density and ice content, respectively), middle (3-6 m, 11 and 7 cores) and bottom sections (3-6 m, 8 and 6 cores) of the firn cores near the summit area (Figure 1). Core CampXV_58 is not included in the figure: the mean density for the top section is 448 kg m^{-3}, and the ice content for the top and middle sections are 3.1% and 15.8%, respectively. The sections are depths below the snow surface, i.e. snow is included in the top sections. Glacier ice is not included in any of the cores; the bottom sections of cores J_99 and X_99 only include depths until −8.7 and −8.8 m, respectively.

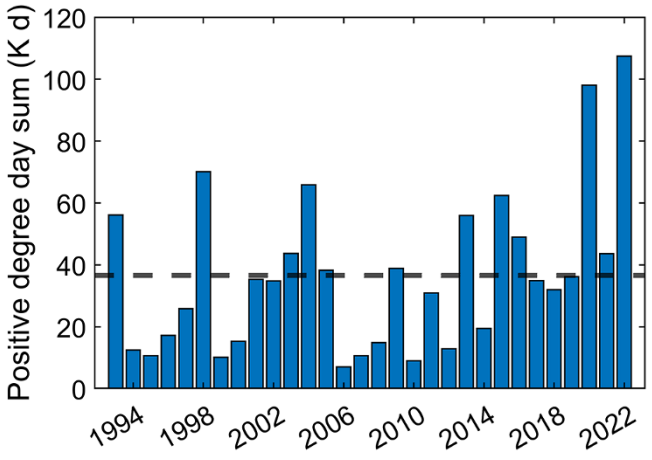

Figure 10. Positive degree day sum from 1993 to 2022 based on mean daily air temperature from the CARRA forcing at site Camp. The dashed line indicates the mean of the 30-year period.

to be increasing in duration and thickness over time. The intermittent depletion and thinning of the aquifers may result from refreezing and/or drainage. Refreezing appears to have contributed to the depletion of the thin aquifer in 2013, with refreezing peaking notably in 2013 (Fig. 8). However, when the firn above the ice-firn interface remains temperate from 2016 onward, thinning and depletion are mainly attributed to lateral drainage, which is governed by the runoff time scale (see Supplementary equation S10). We note that the model does not account for englacial water transport, such as firn aquifer water draining through cracks or crevasses (Poinar and others, 2017; Cicero and others, 2023), which would contribute to decreased aquifer thickness.

Arkhipov and others (1987) and Zagorodnov and others (1989) reported evidence of year-around water in firn at the summit of Austfonna in the 1980s, inferred from borehole drillings in the summers of 1984, 1985 and 1987. However, high spatial variability was observed, with cold firn detected near boreholes with water incursions, indicating water pooling in local depressions. It remains unclear whether these local firn aquifers persisted over time or were episodic, short-lived phenomena facilitated by the abnormally warm summers in 1985 and 1986 (Zagorodnov and others, 1989). However, at least at site Camp, our observations and simulations from 2009 to 2022 indicate a general transition from cold to temperate conditions, along with the emergence of firn aquifers.

The formation of perennial firn aquifers is highly dependent on climatic drivers, particularly accumulation rate and liquid water input. Previous studies simulating conditions conducive to the formation of perennial firn aquifers have primarily focused on Greenland (Forster and others, 2014; Munneke and others, 2014; Miège and others, 2016; Brils and others, 2024). They conclude that accumulation must be high enough to provide the pore space needed for water storage while preventing refreezing, and that melt and rain must be sufficient to enable aquifer formation. It has been suggested that an aquifer region could turn into an ice slab region when liquid water input increases (Brils and others, 2024). Further research is needed to better understand the conditions controlling the formation and extent of firn aquifers in Svalbard glaciers, where high-elevation accumulation zones typically have temperate deep firn (van Pelt and others, 2019). A strong easterly-westerly climatic gradient in Svalbard (Schuler and Østby, 2020) and, for example, the largely asymmetric accumulation pattern on Austfonna (e.g. Dunse and others, 2009) would be interesting study targets for examining the impact of climatic conditions on the extent of aquifers.

5.4. Refreezing

Previous Svalbard-wide modeling studies report decreasing trends in refreezing, mainly attributed to a reduction in firn area (Østby and others, 2017; van Pelt and others, 2019; Noël and others, 2020). In contrast, our study simulates refreezing at a single location, where changes reflect available pore space, cold content, and surface water input, independent of glacier-wide firn area reductions. We do not find a statistically significant trend in refreezing in the top 10 m firn layer between 2009 and 2022, despite a decreasing trend in pore space (Fig. 8). This suggests an increase in meltwater and rain that can refreeze due to a sufficient build-up of cold content during winter. However, refreezing is expected to decrease in the future at our simulation site as firn thickness, cold content,

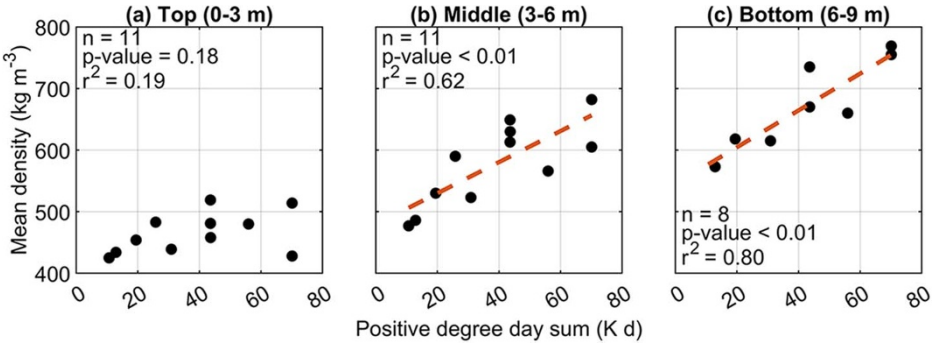

Figure 11. Positive degree day sum and mean density of the (a) top (0-3 m, 11 cores), (b) middle (3-6 m, 11 cores), and (c) bottom (6-9 m, 8 cores) sections. The PDD sum is from the year prior to core retrieval. The dashed line is the linear fit (only shown when significant; p-value < 0.05). The p-value is the probability value, and r^2 is the coefficient of determination. The significance is evaluated at a 95% confidence level.

and available pore space decline due to increased melt and negative annual mass balances (van Pelt and others, 2021). Our results indicate that the turning point at which refreezing decreases has not yet been reached in the summit area of Austfonna. However, interannual variability in refreezing is large (Noël and others, 2020), and Schuler and others (2020) suggest that the region-wide turning point might not be as clearly discernible in Svalbard glaciers as in the peripheral glaciers of Greenland (Noël and others, 2017).

6. Conclusions

Sixteen firn cores drilled on the Austfonna ice cap between 1958 and 2022 are characterized by frequent ice layers, even in the summit area, but ice slabs (>1 m ice layers) that are found in other regions, such as western and northern Greenland (MacFerrin and others, 2019) and the Canadian Arctic (Bezeau and others, 2013) are absent. Ice content and density appear generally lower in core sections 3-6 m below the surface between 2010 and 2015 compared to earlier and later, consistent with lower melt amounts inferred from positive degree-day calculations. However, no clear trends in time or elevation are observed.

Firn temperature observations near the summit between 2009 and 2022 uncover a shift in the thermal regime of the firn. In 2013, the firn above the firn-ice interface transitioned from cold to temperate year-round. This suggests enhanced warming of the deeper firn layers due to increased latent heat release from refreezing, with insufficient winter cooling to offset it. We used the CryoGrid community model, validated against in situ surface mass balance, temperature, and density data, to simulate firn temperature, water content, and density. The model simulations support the observed thermal shift in 2013 and also the repeated formation of firn aquifers since then.

Direct observations such as firn drilling and ground-penetrating radar surveys would be beneficial for confirming the inferred presence of a firn aquifer at site Camp, as well as determining its thickness and extent. Additionally, direct observations of firn thickness are necessary to improve model simulations. Further investigations are also needed to assess the impact of these firn aquifers on the mass balance of the ice cap.

Supplementary material. The supplementary material for this article can be found at https://doi.org/10.1017/jog.2025.10072.

Author contributions. SI gathered, compiled, quality-controlled and curated the datasets, performed the data analyses and simulations, and generated the figures. SI, RH and TVS initiated and designed the study. TVS, and, in particular RH, provided overall guidance throughout this work. SI interpreted the results with significant input from RH, FC and TVS, and wrote the manuscript with contributions from all co-authors, in particular RH. LSS, FC and TVS assisted with figure visualization. LSS adapted the CryoGrid model code in direct collaboration with SI and assisted considerably with the simulations. SI led the firn core fieldwork in 2022 with support from GM. TVS and GM collected and provided other field data. All authors commented on and contributed to the clarity of the manuscript.

Acknowledgements. Fieldwork on Austfonna has been supported by ESA project CryoVEx (PEA no 4000110725), the Research Council of Norway projects AltiMelt (grant 251355/F50) and SIOS-InfraNor (grant 269927). Further work has been supported by the Research Council of Norway through the Nansen Legacy project (grant 276730).

SI was supported by Maa- ja Vesitekniikan Tuki Ry (scholarship 4438). RH was supported by the Research Council of Norway (project 324131) and ERC-2022-ADG grant 101096057 (GLACMASS).

We thank the Norwegian Polar Institute for the logistic support and Eirik Hellerud for assistance in the field in 2022. We are grateful to Takao Kameda and Hideaki Motoyama for providing previously published firn core data in digital form. Jon Ove Hagen, Elisabeth Isaksson, and Lisbeth Langhammer provided valuable information in locating previously unpublished firn data. Veijo Pohjola gave insightful comments on this work. We thank two anonymous reviewers and the editor Dr. William Colgan for their valuable contributions to the manuscript.

Data and software availability. The version of the CryoGrid code used for this study is available at https://doi.org/10.5281/zenodo.15838031. The firn core data are available at https://doi.org/10.21334/NPOLAR.2025.9A2A014B. The firn temperature data are available at https://doi.org/10.21334/NPOLAR.2025.10DB6623. The surface mass balance data are available at https://mosj.no/en/indikator/climate/land/mass-balance-for-glaciers-in-svalbard/.

References

Aas KS and 6 others (2016) The climatic mass balance of Svalbard glaciers: a 10-year simulation with a coupled atmosphere–glacier mass balance model. *The Cryosphere* **10**(3), 1089–1104. doi: 10.5194/tc-10-1089-2016

Arkhipov S and 11 others (1987) Soviet glaciological investigations on Austfonna, Nordaustlandet, Svalbard in 1984-1985. *Polar Geography* **11** 25–49. doi: 10.1080/10889378709377309

Bezeau P, Sharp M, Burgess D and Gascon G (2013) Firn profile changes in response to extreme 21st-century melting at Devon Ice Cap, Nunavut, Canada. *Journal of Glaciology* **59**(217), 981–991. doi: 10.3189/2013JoG12J208

Braithwaite RJ, Laternser M and Pfeffer WT (1994) Variations of near-surface firn density in the lower accumulation area of the Greenland ice sheet, Pâkitsoq, West Greenland. *Journal of Glaciology* **40**(136), 477–485. doi: 10.3189/S002214300001234X

Brils M and 6 others (2024) Climatic drivers of ice slabs and firn aquifers in Greenland. *Geophysical Research Letters* **51**(3), e2023GL106613. doi: 10.1029/2023GL106613

Christianson K, Kohler J, Alley RB, Nuth C and van Pelt WJJ (2015) Dynamic perennial firn aquifer on an Arctic glacier. *Geophysical Research Letters* **42**(5), 1418–1426. doi: 10.1002/2014GL062806

Cicero E and 6 others (2023) Firn aquifer water discharges into crevasses across Southeast Greenland. *Journal of Glaciology* **69**(277), 1379–1392. doi: 10.1017/jog.2023.25

Cogley J and 10 others (2011) Glossary of Glacier Mass Balance and Related Terms, IHP-VII Technical Documents in Hydrology No. 86. Technical report Paris.

Culberg R, Schroeder DM and Chu W (2021) Extreme melt season ice layers reduce firn permeability across Greenland. *Nature Communications* **12**(1), 2336–2336. doi: 10.1038/s41467-021-22656-5

Dowdeswell J and 5 others (1986) Digital mapping of the Nordaustlandet ice caps from airborne geophysical investigations. *Annals of Glaciology* **8**, 51–58. doi: 10.3189/S0260305500001130

Dunse T and 5 others (2013) *Ground-Based Monitoring of Firn Extent and Thickness of Austfonna, Svalbard, to Enhance Interpretation of Satellite-Derived Altimetry Data*. Obergurgl, Austria: IASC Network on Arctic Glaciology, ISBN 978-90-393-6003-3.

Dunse T and 5 others (2015) Glacier-surge mechanisms promoted by a hydro-thermodynamic feedback to summer melt. *The Cryosphere* **9**(1), 197–215. doi: 10.5194/tc-9-197-2015

Dunse T and 5 others (2009) Recent fluctuations in the extent of the firn area of Austfonna, Svalbard, inferred from GPR. *Annals of Glaciology* **50**(50), 155–162. doi: 10.3189/172756409787769780

Forster RR and 12 others (2014) Extensive liquid meltwater storage in firn within the Greenland ice sheet. *Nature geoscience* **7**(2), 95–98. doi: 10.1038/ngeo2043

Fürst JJ and 25 others (2018) The ice-free topography of Svalbard. *Geophysical Research Letters* **45**(21), 11760–11769. doi: 10.1029/2018GL079734

Gascon G, Sharp M, Burgess D, Bezeau P and Bush ABG (2013) Changes in accumulation-area firn stratigraphy and meltwater flow during a period of climate warming: Devon Ice Cap, Nunavut, Canada. *Journal of Geophysical Research: Earth Surface* **118**(4), 2380–2391. doi: 10.1002/2013JF002838

Geyman EC, van Pelt WJJ, Maloof AC, Aas HF, and Kohler J (2022) Historical glacier change on Svalbard predicts doubling of mass loss by 2100. *Nature (London)* **601**(7893), 374–379. doi: 10.1038/s41586-021-04314-4

Harper J, Humphrey N, Pfeffer WT, Brown J and Fettweis X (2012) Greenland ice-sheet contribution to sea-level rise buffered by meltwater storage in firn. *Nature* **491**(7423), 240–243. doi: 10.1038/nature11566

Hock R and 7 others (2019) GlacierMIP – A model intercomparison of global-scale glacier mass-balance models and projections. *Journal of Glaciology* **65**(251), 453–467. doi: 10.1017/jog.2019.22

Horlings AN, Christianson K, and Miège C (2022) Expansion of firn aquifers in Southeast Greenland. *Journal of Geophysical Research: Earth Surface* **127**(10), e2022JF006753. doi: 10.1029/2022JF006753

Irvine-Fynn TDL, Hodson AJ, Moorman BJ, Vatne G and Hubbard AL (2011) Polythermal glacier hydrology: A review. *Reviews of Geophysics* **49**(4), 2010RG000350. doi: 10.1029/2010RG000350

Isaksen K and 5 others (2016) Recent warming on Spitsbergen–Influence of atmospheric circulation and sea ice cover. *Journal of Geophysical Research: Atmospheres* **121**(20), 11913–11931. doi: 10.1002/2016JD025606

Jullien N, Tedstone AJ, Machguth H, Karlsson NB and Helm V (2023) Greenland ice sheet ice slab expansion and thickening. *Geophysical Research Letters* **50**(10), e2022GL100911. https://doi.org/10.1029/2022GL100911

Langhammer L (2014) *Application and evaluation of a borehole camera system for mapping firn stratigraphy.* Master's thesis, University of Oslo.

Lefauconnier B and Hagen JO (1991) *Surging and Calving Glaciers in Eastern Svalbard*. Meddelelser 116. Oslo, Norway: Norwegian Polar Institute.

MacFerrin M and 13 others (2019) Rapid expansion of Greenland's low-permeability ice slabs. *Nature* **573**(7774), 403–407. doi: 10.1038/s41586-019-1550-3

Machguth H and 9 others (2016) Greenland meltwater storage in firn limited by near-surface ice formation. *Nature Climate Change* **6**(4), 390–393. doi: 10.1038/nclimate2899

Mannerfelt ES, Schellenberger T and Kääb AM (2025) Tracking glacier surge evolution using interferometric SAR coherence–examples from Svalbard. *Journal of Glaciology* **71**, e43. doi: 10.1017/jog.2025.27

Marchenko S and 7 others (2017a) A plot-scale study of firn stratigraphy at Lomonosovfonna, Svalbard, using ice cores, borehole video and GPR surveys in 2012–14. *Journal of Glaciology* **63**(237), 67–78. doi: 10.1017/jog.2016.118

Marchenko S and 6 others (2017b) Parameterizing deep water percolation improves subsurface temperature simulations by a multilayer firn model. *Frontiers in Earth Science* **5**. doi: 10.3389/feart.2017.00016

Miège C and 12 others (2016) Spatial extent and temporal variability of Greenland firn aquifers detected by ground and airborne radars. *Journal of Geophysical Research: Earth Surface* **121**(12), 2381–2398. doi: 10.1002/2016JF003869

Moholdt G and Kääb A (2012) A new DEM of the Austfonna ice cap by combining differential SAR interferometry with ICESat laser altimetry. *Polar Research* **31**(1), 18460. doi: 10.3402/polar.v31i0.18460

Montgomery L and 8 others (2020) Hydrologic properties of a highly permeable firn aquifer in the Wilkins Ice Shelf, Antarctica. *Geophysical Research Letters* **47**(22), e2020GL089552. doi: 10.1029/2020GL089552

Munneke PK, Ligtenberg SRM, van den Broeke MR, van Angelen JH and Forster RR (2014) Explaining the presence of perennial liquid water bodies in the firn of the Greenland Ice Sheet. *Geophysical Research Letters* **41**(2), 476–483. doi: 10.1002/2013GL058389

Noël B and 9 others (2017) A tipping point in refreezing accelerates mass loss of Greenland's glaciers and ice caps. *Nature Communications* **8**(1), 14730–14730. doi: 10.1038/ncomms14730

Noël B and 10 others (2020) Low elevation of Svalbard glaciers drives high mass loss variability. *Nature Communications* **11**(1), 4597–4597. doi: 10.1038/s41467-020-18356-1

Nordli Ø, Przybylak R, Ogilvie AE and Isaksen K (2014) Long-term temperature trends and variability on Spitsbergen: The extended Svalbard Airport temperature series, 1898–2012. *Polar Research* **33**(1), 21349. doi:10.3402/polar.v33.21349

Norwegian Polar Institute (2014a) Kartdata Svalbard **1**, 100 000 S100 (Kartdata) / Map Data [Data set]. doi: 10.21334/npolar.2014.645336c7

Norwegian Polar Institute (2014b) Terrengmodell Svalbard (S0 Terrengmodell). doi: 10.21334/npolar.2014.dce53a47

Nuth C and 7 others (2013) Decadal changes from a multi-temporal glacier inventory of Svalbard. *The Cryosphere* **7**(5), 1603–1621. doi: 10.5194/tc-7-1603-2013

Østby TI, Schuler TV, Hagen JO, Hock R, Kohler J and Reijmer CH (2017) Diagnosing the decline in climatic mass balance of glaciers in Svalbard over 1957–2014. *The Cryosphere* **11**(1), 191–215. doi: 10.5194/tc-11-191-2017

Pfeffer WT, Meier MF and Illangasekare TH (1991) Retention of Greenland runoff by refreezing: Implications for projected future sea level change. *Journal of Geophysical Research: Oceans* **96**(C12), 22117–22124. doi: 10.1029/91JC02502

Pinglot JF, Hagen JO, Melvold K, Eiken T and Vincent C (2001) A mean net accumulation pattern derived from radioactive layers and radar soundings on Austfonna, Nordaustlandet, Svalbard. *Journal of Glaciology* **47**(159). doi: 10.3189/172756501781831800

Poinar K and 5 others (2017) Drainage of Southeast Greenland Firn Aquifer Water through Crevasses to the Bed. *Frontiers in Earth Science* **5**. doi: 10.3389/feart.2017.00005

Rennermalm ÅK and 12 others (2022) Shallow firn cores 1989–2019 in southwest Greenland's percolation zone reveal decreasing density and ice layer thickness after 2012. *Journal of Glaciology* **68**(269), 431–442. doi: 10.1017/jog.2021.102

Schmidt LS, Schuler TV, Thomas EE and Westermann S (2023) Meltwater runoff and glacier mass balance in the high Arctic: 1991–2022 simulations for Svalbard. *The Cryosphere* **17**(7), 2941–2963. doi: 10.5194/tc-17-2941-2023

Schuler TV and 12 others (2020) Reconciling Svalbard Glacier Mass Balance. *Frontiers in Earth Science* **8**. doi: 10.3389/feart.2020.00156

Schuler TV, Dunse T, Østby TI and Hagen JO (2014) Meteorological conditions on an Arctic ice cap – 8 years of automatic weather station data from Austfonna, Svalbard. *International Journal of Climatology* **34**(6), 2047–2058. doi: 10.1002/joc.3821.

Schuler TV and 5 others (2007) Calibrating a surface mass-balance model for Austfonna ice cap, Svalbard. *Annals of Glaciology* **46**, 241–248. doi: 10.3189/172756407782871783

Schuler TV and Østby TI (2020) Sval_Imp: A gridded forcing dataset for climate change impact research on Svalbard. *Earth System Science Data* **12**(2), 875–885. doi: 10.5194/essd-12-875-2020

Schyberg H and 30 others (2020) Arctic regional reanalysis on single levels from 1991 to present. *Copernicus Climate Change Service (C3S) Climate Data Store (CDS)*. doi: 10.24381/cds.713858f6

Schytt V (1964) Scientific Results of the Swedish Glaciological Expedition to Nordaustlandet, Spitsbergen, 1957 and 1958. *Geografiska Annaler* **46**(3), 242–281. doi: 10.2307/520382

Taurisano A and 6 others (2007) The distribution of snow accumulation across the Austfonna ice cap, Svalbard: Direct measurements and modelling. *Polar Research* **26**(1), 7–13. doi: 10.1111/j.1751-8369.2007.00004.x

van den Akker T, van Pelt W, Petterson R, and Pohjola VA (2025) Long-term development of a perennial firn aquifer on the Lomonosovfonna ice cap, Svalbard. *The Cryosphere* **19**(4), 1513–1525. doi: 10.5194/tc-19-1513-2025

van Pelt W and 10 others (2019) A long-term dataset of climatic mass balance, snow conditions, and runoff in Svalbard (1957–2018). *The Cryosphere* **13**(9), 2259–2280. doi: 10.5194/tc-13-2259-2019

van Pelt WJJ, Schuler TV, Pohjola VA and Pettersson R (2021) Accelerating future mass loss of Svalbard glaciers from a multi-model ensemble. *Journal of Glaciology* **67**(263), 485–499. doi: 10.1017/jog.2021.2

Vionnet V and 7 others (2012) The detailed snowpack scheme Crocus and its implementation in SURFEX v7.2. *Geoscientific Model Development* **5**(3), 773–791. doi: 10.5194/gmd-5-773-2012.

Watanabe O and 7 others (2001) Studies on climatic and environmental changes during the last few hundred years using ice cores from various sites in Nordaustlandet, Svalbard (scientific paper). *Memoirs of National Institute of Polar Research Special Issue* **54**.

Westermann S and 23 others (2023) The CryoGrid community model (version 1.0) – A multi-physics toolbox for climate-driven simulations in the terrestrial cryosphere. *Geoscientific Model Development* **16**(9), 2607–2647. doi: 10.5194/gmd-16-2607-2023

Wilson NJ and Flowers GE (2013) Environmental controls on the thermal structure of alpine glaciers. *The Cryosphere* **7**(1), 167–182. doi: 10.5194/tc-7-167-2013

Xiao J and 7 others (2022) Local-scale spatial variability in firn properties in Southwest Greenland. *Frontiers in Earth Science* **10**. doi: 10.3389/feart.2022.938246

Zagorodnov V, Sinkevich S and Arkhipov S (1989) Hydrothermal regime of the ice-divide area of Austfonna, Nordaustlandet [In Russian with English summary]. *Data of Glaciological Studies* **68**, 133–141.

Zdanowicz C and 6 others (2012) Summer melt rates on Penny Ice Cap, Baffin Island: Past and recent trends and implications for regional climate. *Journal of Geophysical Research: Earth Surface* **117**(F2), F02006. doi: 10.1029/2011JF002248

Zweigel RB and 6 others (2021) Simulating Snow Redistribution and its Effect on Ground Surface Temperature at a High-Arctic Site on Svalbard. *Journal of Geophysical Research: Earth Surface* **126**(3) e2020JF005673. doi: 10.1029/2020JF005673